# Tracking mechanics and volume of globular cells with atomic force microscopy using a constant-height clamp

Martin P Stewart[1,2], Yusuke Toyoda[2], Anthony A Hyman[2] & Daniel J Müller[1]

[1]ETH Zurich, Department of Biosystems Science and Engineering, Basel, Switzerland. [2]Max Planck Institute of Molecular Cell Biology and Genetics, Dresden, Germany. Correspondence should be addressed to D.M. (daniel.mueller@bsse.ethz.ch).

Published online 5 January 2012; doi:10.1038/nprot.2011.434

**To understand the role of physical forces at a cellular level, it is necessary to track mechanical properties during cellular processes. Here we present a protocol that uses flat atomic force microscopy (AFM) cantilevers clamped at constant height, and light microscopy to measure the resistance force, mechanical stress and volume of globular animal cells under compression. We describe the AFM and cantilever setup, live cell culture in the AFM, how to ensure stability of AFM measurements during medium perfusion, integration of optical microscopy to measure parameters such as volume and track intracellular dynamics, and interpretation of the physical parameters measured. Although we use this protocol on trypsinized interphase and mitotic HeLa cells, it can also be applied to other cells with a relatively globular shape, especially animal cells in a low-adhesive environment. After a short setup phase, the protocol can be used to investigate approximately one cell per hour.**



## INTRODUCTION

### Forces in cells

Physical forces are crucial to a number of cellular processes such as cell division[1,2], stem cell differentiation[3], cell migration[4–6], tissue formation[7,8] and development[9,10], wound healing[11], tumor growth[12,13], progression of disease states[14–21], biomechanics[22] and mechanotransduction[23]. In all of these processes, forces must be generated and transmitted through the components of the cells themselves, and therefore it is crucial to understand the mechanical properties of the cell. Mechanical properties can be assessed by studying the relationship between stress (force/area) and strain (deformation) as a function of time[24]. These concepts, which were originally developed from materials science and engineering of inanimate materials, have been adapted to the cellular context[25].

### Historical beginnings of cell mechanics

Some of the first single-cell micromechanical studies were carried out on the relatively large (diameter ~100 μm) egg cells of marine and amphibian organisms. Methods involved the sessile drop approach[26], centrifuge microscopy[27,28], compression with microbeams[29] and microplates[30,31], micropipette aspiration[32,33], microneedle poking[34] and tensile stretching with beads[35]. These pioneering efforts inspired studies on the much smaller and more delicate red blood cells; these studies exploited technological improvements in microscopy and mechanical techniques such as micropipette aspiration[36,37] and fluid shear stress assays[38]. From the results of these studies, researchers made apparent the connection between the mechanical properties of individual blood cells and their contribution to pathophysiology[39,40], and these effects are currently well documented[41].

### A diversity of methods in cell mechanics

After these promising beginnings, the challenge was to expand the field of animal cell mechanics to cover a broader range of cell types and biological contexts[42]. At present, progress has been enabled by the development and optimization of techniques to measure and apply forces and displacements with picoNewton and nanometer sensitivity in combination with enhanced live cell microscopy[43]. Methods currently in use can be roughly split into two categories. The first category involves active imposition of force or deformation on the cell and includes micropipette aspiration[44], parallel plate devices[45,46], magnetic twisting cytometry[47,48], active microrheology[49], optical tweezers[50–52], optical cell stretching[53], cell-populated substrate or gel deformation devices[54,55], fluid shear stress[56,57], microfluidics[58,59], micro-electro-mechanical systems[60,61] and various modes of AFM[62–67]. The second category of methods instead teases out mechanical information from optical or acoustic data and includes passive microrheology by tracking probe particles[49] or subcellular components[68,69], analysis of contractile release dynamics[70,71], acoustic microscopy[72,73], laser ablation of subcellular structures[74], optical mapping of intracellular force distribution[75] and traction force microscopy in two dimensions using deformable substrates[76,77] and flexible micropillar arrays[78,79] or in three dimensions with elastic gel matrices containing embedded fiduciary markers[80,81]. In general, the first category of techniques is more straightforward and involves fewer assumptions, whereas the second category involves substantial computational and data analysis but has a better capability to probe beyond the surface.

### AFM in cell mechanics

Of all the above-mentioned techniques, one of the most versatile is AFM, which provides a multifaceted platform to the study forces and mechanics in cell biology. Commercial AFM instruments designed for biological research are becoming increasingly adaptable and include cell-friendly options such as temperature control, liquid perfusion and compatibility with high-end light microscopes. Moreover, the experimental procedure can be tailored to probe local or global mechanical properties of cells over a wide range of forces from picoNewtons to microNewtons at nanometer precision, and it can provide high temporal resolution

ranging from microseconds to hours. The cantilever can be made to perform rapid indentations, long-timescale deformations or oscillations over various frequencies to extract rheologically relevant moduli. For example, mechanical measurements can be made locally by using pyramidal or spherical tips to indent the cell[62,82–84] or by subjecting it to oscillations of varying frequency[63–66]. Alternatively, global cell measurements can be made by using flat cantilevers to perform whole-cell compression[67,85,86], stretching[67] or oscillatory deformation[87] experiments. Apart from traditional mechanics, other innovative AFM methods have been developed to quantify, for example, cell adhesion forces down to single receptor level[88,89] and the forces of cell motility[90]. Moreover, AFM is also a valuable tool to probe the nanomechanics of biomolecules, such as individual proteins, which may be important in cellular mechanics[43,91,92]. Notwithstanding these benefits, disadvantages of most AFM-based methods in cell mechanics often include the time-consuming and low-throughput nature of single-cell experiments and the inability to probe beneath the cell surface.

## AFM to probe the mechanics and volume of mitotic cells

Here we present an AFM-based protocol that was recently used to characterize the forces that drive mitotic cell rounding[85]. Mitotic cell rounding involves the transition of a cell from a flat or elongated shape into a round state when passing through the cell cycle from G2 into mitosis (M), and occurs on both 2D substrates and in 3D tissue environments. We originally started investigating the mechanics of G2/M cells by imposing constant forces with soft, flat cantilevers having spring constants $k$ = 30–50 mN m$^{-1}$; however, they could neither measure nor apply forces over 20 nN, and thus we selected stiffer cantilevers ($k$ = 200–500 mN m$^{-1}$) that provide a force range from tens of picoNewtons to hundreds of nanoNewtons. Moreover, we wanted to monitor cell size, and thus we customized our assay to constrain cells to a constant height and therefore impose a near-uniform cylindrical shape on the cell. The use of light microscopy to track the cross-sectional area of cells enabled the estimation of cell volume. In these experiments, we imposed on cells a compressive strain of ~50% and measured the response force, mechanical stress or 'rounding pressure' (force/area) and volume of G2/M cells. We found that cells markedly increased their pressure on entering mitosis, as the resistance force against the cantilever increased approximately threefold within ~10 min without any substantial changes in cell size[85]. By tracking pressure and volume simultaneously, we were able to dissect distinct roles for both osmotic pressure and the actomyosin cortex (a contractile layer of actin filaments and myosin motors located underneath the plasma membrane) in this force-generation process. Compromising the cellular ability to generate osmotic pressure caused cell shrinkage and softening, whereas abolishing the actomyosin cortex caused volume increase and softening of the cell. Monitoring the volume of the cells was key in these experiments, as it enabled us to observe how the forces acted on the fluid fraction of the cell (i.e., actomyosin contraction pulling inward and osmotic pressure pushing outward). The actomyosin system had previously been recognized in the mechanics of mitotic cell rounding[93–96] and cell mechanics in general; however, the role of osmotic pressure had not been extensively tested. We showed that the actomyosin cortex can be deployed in a similar role to a plant or bacterial cell wall, and thus maintain an osmotic pressure. In such a scenario, the balance between actomyosin contraction and osmotic pressure would be sufficient to control cell mechanics and shape.

### Protocol purpose and description

The primary purpose of this protocol is to simultaneously track the mechanical properties and volume of globular cells. Here we demonstrate the setup on round mitotic cells (**Fig. 1**). A candidate cell is vertically deformed ~50% by a flat tipless cantilever as the AFM continuously records the response force (**Fig. 1b**). This is essentially a stress-relaxation assay in materials science terms: a constant deformation is imposed on a material sample and the response stress is monitored over time[24]. Transmission and/or fluorescence light microscopy are used to measure cell dimensions (**Fig. 1c**). By taking the measured forces and cellular dimensions and applying the relationships shown in **Figure 1d**, we can calculate cell volume and response stress or rounding pressure. In the context of mitotic cells, we refer to the response stress as rounding pressure because these forces must drive mitotic cell rounding in a tightly packed tissue environment. If cell deformation is close to constant, then the measured pressure (force/area) is almost proportional to the elastic modulus, a convenient mechanical boundary condition for this protocol. Therefore, we recommend first using stiff cantilevers (at least 300 mN m$^{-1}$ in this protocol) if large force changes (tens of nanoNewtons) are expected and second imposing large cellular deformations (~50%) if substantial volume changes are anticipated. This is shown in **Figure 2a** with the case of a round cell that changes in volume by 20%. With a constant-height clamp vertically deforming the cell height by 10%, a 20% volume decrease or increase of the cell causes the vertical deformation changing to 3% or 15.3%, respectively ((i) in **Fig. 2a**). However, with a 50% cell height deformation, the same volume alterations cause vertical deformation to only change to 46.1% and 52.9%, respectively ((ii) in **Fig. 2a**). Therefore, a constant-height clamp with a larger initial deformation is better at holding deformation closer to a constant value during cell volume changes. Moreover, a constant-height clamp vertically deforming the cell by 50% increases the sensitivity of volume change detection with light microscopy in the horizontal dimensions (**Fig. 2a**). For these reasons, it is preferable to produce a larger original deformation in an experiment where the researcher expects a volume change during a cellular process. Importantly, such deformations do not inhibit cells from proceeding through mitosis in normal time or markedly alter the cell mechanics[85]. Moreover, cells in real tissues are not mechanically isolated as in *in vitro* cell culture, and therefore this method represents a way of simulating the constraints of real tissue or examining the effect of various imposed forces and deformations.

### Comparison with other AFM methods

In the early 1990s, researchers began using AFM to indent soft biological samples with commonly available sharp pyramidal tips[97] and to approximate mechanical properties by exploiting Hertzian model[98] with Sneddon's modifications[99]. These advancements were adapted to live cells in physiological medium[100]. The high spatial resolution attainable with sharp AFM tips enabled force-volume measurements that probe the cell surface with vertical force-distance indentations (**Fig. 2b**), providing cell height and stiffness for each sampled point[101,102]. The cell height at each point can be summed up to determine a spatial map of cell volume and stiffness of the cell surface. However, pyramidal tips indenting (up to several μm)

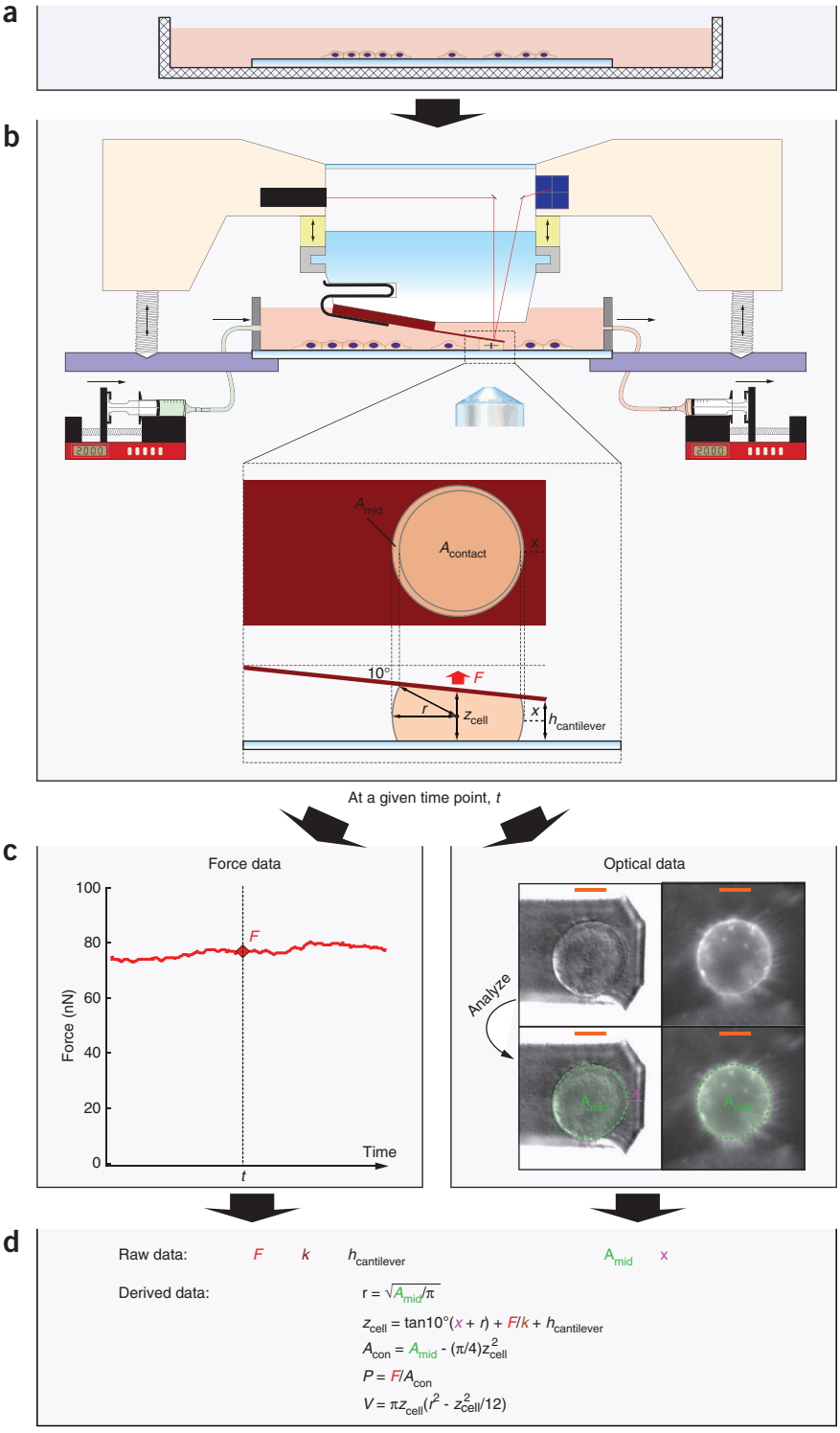


**Figure 1** | Overview of the protocol. (**a**) Cell preparation: cells are seeded onto a 24-mm glass cover slip as detailed in REAGENT SETUP. (**b**) Experimental setup: a schematic of the AFM setup and a mitotic HeLa cell as it is confined under a flat tipless AFM cantilever. Cantilever deflection is measured with the AFM laser-based optical lever principle and converted to a force via parameters established through standard calibration procedures. The cantilever is held in place flush with the 10° angle of the glass block using a metal spring clip (black). The glass block is secured into the AFM head below the piezoelectric actuator with a twist-lock system. A window within the AFM head facilitates transmission light microscopy. Coarse motors (screw legs) vertically position the AFM head within range of the substrate. Fine piezoelectric movements (yellow element) control the movement of the glass black and cantilever chip combination during AFM experiments. Push-pull pump setups can be used to exchange media during live cell experiments, and therefore expose the cell to various perturbations. A diagram of the confined cell with details of its associated geometry is shown in the dashed box. (**c**) Data extraction: the raw data captured in this protocol include continuously sampled force data and intermittently acquired optical images. At any time point *t*, optical images can be used to determine the geometry. (**d**) Data analysis: along with force, these parameters can be used to calculate rounding pressure (*P*) and volume (*V*). Symbols are force (*F*), spring constant of the cantilever as determined by calibration (*k*), set height of the cantilever ($h_{cantilever}$), height of the middle of the cell ($z_{cell}$), radius of the cell (*r*), area of the mid section of the cell ($A_{mid}$), cell-cantilever contact area ($A_{con}$) and distance from the free end of the cantilever to the edge of the cell (*x*).



the cell surface were found to induce mechanical artifacts and overestimate stiffness due to uncertainties in contact point, contact area, strain estimations and questionable assumptions regarding cell properties such as material homogeneity, Poisson's ratio and tip-sample interaction[82,103]. Some of these problems were alleviated by switching to spherical tips (**Fig. 2c**), which have become the standard[83,84,103,104]. Nevertheless, local indentation techniques may struggle to describe the dynamic and heterogeneous complexity of processes affecting the entire cell but, on the other hand, offer enhanced spatial resolution. This contrasts with measurements that achieve a whole cell readout of force or stress without the aid of sophisticated models. However, to adequately probe mechanical properties of the entire cell (and not only of the cell surface or plasma membrane) requires substantial deformations regardless of the AFM technique.

The features of AFM-based methods for analyzing cell mechanics and volume of different cell shapes are shown in comparison with our protocol in **Figure 2**. Flat tipless cantilevers have been used to measure whole-cell mechanics[67,86] or mechanics and volume simultaneously[85]. Because of the tipless geometry of the AFM cantilever, such measurements extract quantitative data preferably from globular or round cells (**Fig. 2b**). However, qualitative assessment of spread cells can also yield biological insights and presents certain advantages such as speed and simplicity[105]. Pyramidal tips perform poorly in cell mechanical measurements[82,103] but are capable

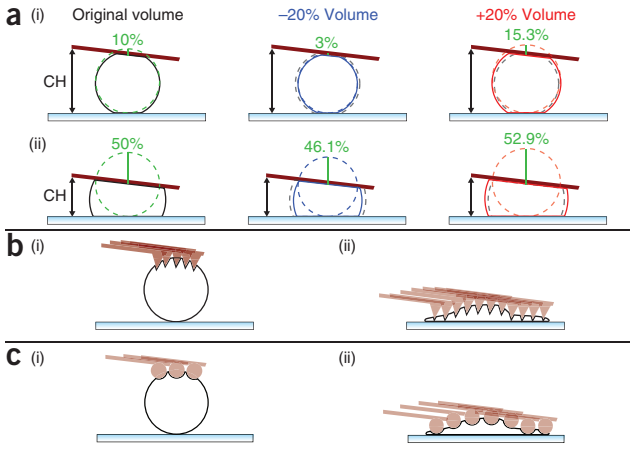


**Figure 2** | AFM-based techniques for cellular mechanics and volume measurements. (**a**) A schematic of cells in an AFM constant-height (CH) clamp assay throughout the course of a volume change. Dashed black cell outlines depict cell size if no volume change had occurred. Dashed colored cell outlines depict cell shape if no cantilever compression or adhesion was present. The vertical deformation of the cell is related to the height of a rounded, unperturbed cell (colored dashed) and to the height of the compressed cell (solid lines). With an initial vertical deformation (green line) of (i) 10%, a cell volume decrease by 20% corresponds to an effective deformation of the cell by 3% and a cell volume increase by 20% corresponds to an effective deformation of the cell by 15.3%. The second case (ii) shows that upon an initial deformation of 50% a cell volume decrease by 20% or increase by 20% becomes an effective volume increase by 46.1% or 52.9%, respectively. (**b**) Schematic of a pyramidal tip probing a round (i) and flat (ii) cell. (**c**) Schematic of a spherical tip probing a round (i) and flat (ii) cell.

of mapping cell volume if cells are flat enough and scan speeds sufficiently slow (a few tens of minutes) to generate clean data ((i) in **Fig. 2b**)[101,102,106]. When applied to round cells, pyramidal tips can only access a portion of the top surface ((ii) in **Fig. 2b**). Spherical tips perform better in local mechanical analysis but do away with the resolution needed for surface scanning and volume maps, and thus only qualitative assessments of cell volume can be made (**Fig. 2c**)[104,107,108]. Both local indentation techniques are limited to probing flat parts (**Fig. 2b,c**) of cells because nonperpendicular loading is beyond the considerations of the models used to interpret the data. Importantly, all these AFM techniques are strong in measuring dimensions in the vertical axis where light microscopy has traditionally been weak. Therefore, AFM in any mode can be applied to round cells in conjunction with light microscopy to determine cell volume at high temporal resolution. Finally, in both volume and mechanics measurements, the same AFM instrument with a different cantilever can potentially be used in a complementary manner to (at least qualitatively) control and confirm observations.

### Applicability of the protocol

This protocol is demonstrated on round mitotic cells but is amenable to the study of most globular-shaped cells, such as cells in nonadherent environments[52,53,59,83,109], nonadherent cells[37,83], cells extracted from widely studied zebrafish and *Caenorhabditis elegans* developmental systems[74,84], and egg cells[29–35]. Notably, investigations on single globular cells have been carried out with parallel plate setups featuring geometry similar to our protocol[30,31,45,46,67,86]. Mechanical methods are becoming increasingly important as part of the investigative toolkit in cell biology because they access mechanical data invisible to conventional light microscopy approaches and they can be combined with RNA interference and chemical genetic approaches to characterize mechanical phenotypes. We believe that the principles underpinning this method may find applications in the clinic for the rapid diagnosis of pathologies related to cell mechanics[16–21,41], and that they will further lead to discoveries at the interface of cell biology, physiology and biophysics.



## MATERIALS

### REAGENTS

- DMEM cell culture medium (1× liquid, GlutaMAX, 4,500 mg per liter D-glucose, sodium pyruvate; Invitrogen, cat. no. 31966-021)
- DMEM powder for reconstitution of AFM medium (10× sachets powder, glutamine, 4,500 mg per liter D-glucose, sodium pyruvate; Invitrogen, cat. no. 12800-017)
- Fetal bovine serum (FBS; Gibco, cat. no. 10270)
- Ethanol (absolute; Merck, cat. no. 1.00983.2511)
- HeLa cells (if you have a strain that expresses GFP-labeled histone (H2B-GFP), this can be helpful for tracking the mitotic phase by fluorescence) **! CAUTION** Follow all relevant ethics guidelines when working with human cells or tissues.
- HEPES (Sigma, cat. no. H3375)
- $NaHCO_3$ (Sigma, cat. no. S6014)
- Ficoll (Sigma, cat. no. F2637)
- Xylose (Sigma, cat. no. 95729)
- Ultrapure water (Purelab Ultra)
- Trypsin-EDTA (0.5% (wt/vol); Gibco, cat. no. 25300)
- PBS with $Ca^{2+}$ and $Mg^{2+}$ (PBS; Gibco, cat. no. 14040-117)
- PBS without $Ca^{2+}$ and $Mg^{2+}$ (PBS; Gibco, cat. no. 14190094)
- Penicillin-streptomycin (100×; Gibco, cat. no. 15140)
- EIPA (5-(*N*-Ethyl-*N*-isopropyl) amiloride; Sigma, cat no. A3085)
- Hoechst 33342

### EQUIPMENT

- BioCell temperature-controlled cover slip holder and liquid incubator (JPK) **▲ CRITICAL** Alternatively, some users may find it more convenient to use a Petri dish holder in conjunction with glass bottom Petri dishes. However, the problem of how to exchange the medium through a Petri dish must be solved by the user. For example, one may insert heated syringe needles through the sides of the Petri dish, connect tubes providing inflowing medium and seal any leaks with vacuum grease.
- Glass cover slips (circular with 24-mm diameter; Marienfeld)
- Nanowizard AFM system (JPK)
- Inverted optical microscope, Axiovision or cell observer (Carl Zeiss)
- Apochromat 20×/0.8 NA objective lens
- Differential interference contrast (DIC) microscope **▲ CRITICAL** Compared with standard bright-field and phase-contrast techniques, transmission DIC microscopy enables improved imaging through the silicon cantilever.
- Tipless silicon AFM cantilevers NSC-12 series (Mikromasch), featuring six different cantilevers labeled A–F per chip. Unless the cantilevers are new, they should be ultrasonically cleaned by mounting in a cantilever holder and subjecting to 2–5% helmanex at 50–60 °C for 5 min, and then thoroughly rinsed with ultrapure water. **▲ CRITICAL** Cantilever choice is an important parameter in these experiments. For long-timescale mechanics experiments, we recommend pure silicon or silicon nitride cantilevers, as metal-coated cantilevers quite frequently suffer from extensive drift because

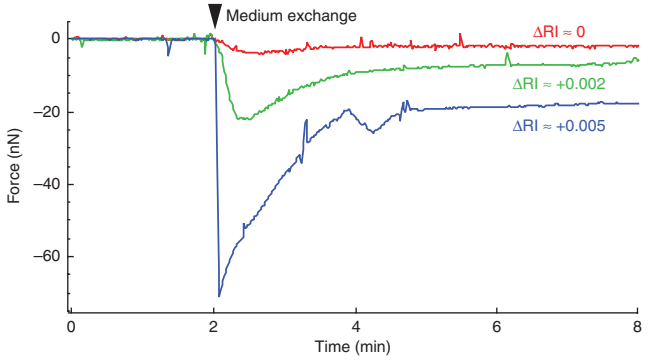


**Figure 3** | Examples of spurious disturbance in force recorded by the AFM setup during exchange of medium with different refractive indices. At time $t$ = 2 min, 2,000-µl medium is exchanged at a flow rate of 2,500 µl $min^{-1}$ while the AFM cantilever hovers ~10 µm above the substrate surface. Spurious disturbance in force can be minimized to a negligible level by reducing the difference in refractive index, ΔRI, between incoming and extant medium.

of the difference between the thermal expansion coefficients of silicon (or silicon nitride) and the metal layer. ▲ **CRITICAL** HeLa cells under significant deformations (≥50%) can be expected to produce resistance forces of ~100 nN. Thus, we recommend using Mikromasch cantilevers D, E or F (Nominal $k$ = 0.35, 0.3, 0.65 N $m^{-1}$, respectively). First, a cantilever that is too soft will deflect the laser beam beyond the range detectable by the AFM optics. Second, a stiffer cantilever is better at maintaining the cell under a state of constant deformation. (A $k$ = 0.3 N $m^{-1}$ cantilever bends ~333 nm at 100 nN).

- Twin Aladdin push-pull pump setup (WPI) ▲ **CRITICAL** The pump and syringe setup should be held at 37 °C in order to prevent thermal drift upon the introduction of perturbing media. For this, we prefer to incubate the whole microscope and surroundings with an incubation system, Cube + Box (Life Imaging Services).
- Luer-Lok syringes (3 ml, BD)
- Microlance 22-G syringe needles (BD)
- Generic plastic tubing with bore to fit 22-G syringe
- ultrapure water source (~18 MΩ $cm^{-1}$, e.g., Purelab Ultra)
- Refractometer

**REAGENT SETUP**

**HeLa cell culture** Maintain HeLa cells in DMEM supplemented with 10% (vol/vol) FBS and 1% (vol/vol) penicillin-streptomycin. To prepare cells for AFM experiments, seed HeLa cells onto 24-mm-diameter glass cover slips. Aim to achieve between 25 and 75% confluence at the time of AFM experiments in order to provide sufficient cells on one hand and enough spaces to measure the height of the substrate on the other hand (see Step 12).

**AFM medium** Each sachet of DMEM powder makes 1 liter of medium. Follow instructions on the packet, which detail how much HEPES and $NaHCO_3$ to be add to the medium. The osmolarity of the medium should be around 300 mOsm $kg^{-1}$. AFM medium is DMEM buffered with HEPES instead of carbonate. A different buffering option is required because, unlike standard incubators for cell culture, the AFM is not enclosed in a 5% $CO_2$ environment. AFM medium can be stored for up to 6 months at 4 °C. If FBS is added, the medium should be consumed within 3 months.

**Hypotonic shock medium** Dilute AFM medium to 200 mOsm $kg^{-1}$ with ultrapure water. ▲ **CRITICAL** It is essential to match the refractive index (RI) of perturbant media to the standard AFM medium, as the introduction of a second liquid with a different RI causes spurious disturbances in the laser-based AFM measurements (**Fig. 3**). Ficoll, which has a negligible effect on osmolarity, can be added to the hypotonic solution until the RI is matched. Addition of 1% (wt/vol) Ficoll increases RI by approximately +0.0013. The RI may be checked with a refractometer.

**AFM medium with EIPA** Make EIPA stock by dissolving EIPA in DMSO, and then dilute into cell medium to achieve the desired concentration. ▲ **CRITICAL** EIPA is an inhibitor of the $Na^+/H^+$ antiporter[110], which we showed to have a role in the mechanics and volume of mitotic cells[85]. The concentration of EIPA used to treat different cells and cell lines will require dose-response trial experiments. Approximately 50 µM was found to be optimal for producing the results using HeLa cells shown in this protocol (see ANTICIPATED RESULTS). ▲ **CRITICAL** When diluting inhibitors dissolved in DMSO into cell medium, it is advisable not to exceed a final concentration of 1% (vol/vol) DMSO because only concentrations < 1% are generally accepted to be nontoxic by the cell biology community. In addition, one must consider that addition of DMSO changes RI by +0.0015 per 1% (vol/vol) DMSO. Once again, as mentioned with the hypotonic medium above, Ficoll, which has negligible effect on osmolarity, can be added to the solution with lower RI until equivalence is achieved.



## PROCEDURE

### Setting up cells in the AFM ● TIMING 1 h

**1|** If you are using an incubator for the AFM setup and light microscope, turn it on at least 4 h before experiments begin. This allows the system to thermally equilibrate.

**2|** Wash all AFM components such as the fluid chamber and glass cantilever holder, which will be in contact with the cell preparation, with detergent; after washing, rinse with ethanol and water and then dry.

**3|** Connect plastic tubing to the inlet and outlet ports of the AFM fluid chamber in preparation for syringe connection.

**4|** Take the cell-populated cover slip (see REAGENT SETUP) and place it in the AFM setup, assemble seals and clamps, and then add sufficient experimental medium (AFM medium, see REAGENTS). For the JPK BioCell, we recommend a volume of ~400 µl. Temperature control systems should be switched on and set to 37 °C. Dry the underside of the cover slip to provide an optically clean surface and avoid crystallization of salts. To prevent evaporation of the cell medium from the fluid chamber during the subsequent setup steps, you may place a glass cover slip or slide over the opening where the cell medium is exposed.

▲ **CRITICAL STEP** During assembly of the seal and clamps, the cells on the cover slip are submerged with very little medium. This step should be completed within 1 min in order to ensure that the cells remain healthy.

### Setting up AFM and cantilever

**5|** Turn on the AFM controller, optical microscope and camera. Start the AFM control software.

**6|** Mount a clean NSC-12 cantilever onto the AFM cantilever-holding block supplied with the AFM. The longer cantilevers (D, E and F) should face out.

**7|** Insert and lock the cantilever holder into the AFM head and position the head on the AFM stage. Place the AFM head on the stage and position the cantilever approximately over the middle of the cover slip to allow maximum space for navigation around the sample. If required, ensure that the required seals are in place to prevent evaporation.

**8|** Start up the light microscopy software and focus on the cantilever. Select the appropriate filters that allow the camera to detect the laser signal. Use the microscopy software to acquire a live image and reduce camera exposure until the laser spot can be seen clearly. Align the laser spot on the end of the cantilever and adjust the photodiode signal according to the guidelines of the AFM manufacturer.

**9|** To begin calibrating the cantilever, first position the cantilever over a blank region on the glass cover slip unpopulated with cells and use the approach program in the AFM software to bring the cantilever within the vicinity of the glass surface. Then, perform extension-retraction cycles against the glass surface and subsequently determine the cantilever sensitivity according to the routines incorporated in the AFM control software.
▲ **CRITICAL STEP** The factor used to convert the volts measured in the AFM photodiode to nanometers of cantilever deflection is usually referred to as sensitivity. It depends on many parameters, including the type of cantilever and how it is mounted. Thus, sensitivity must be determined each time a cantilever is mounted or remounted. To determine sensitivity, an extension-retraction cycle is performed against the hard surface of the glass cover slip. The subsequent force-distance data are used to analyze the deflection of the cantilever when in contact with the glass surface. In this contact region, the deflection of the cantilever is equal to the vertical movement of the AFM piezo element.

**10|** To complete the calibration process, a cantilever spring constant ($k$) must be provided. Use the AFM software to perform thermal noise calibration. In order to avoid surface-induced artifacts, the cantilever must be withdrawn at least 100 µm from the glass cover slip.
▲ **CRITICAL STEP** The parameters established in cantilever calibration are necessary to convert the measured photodiode voltage into a force. First, voltage (V) is multiplied by sensitivity (nm $V^{-1}$) to yield deflection distance (nm), which is in turn multiplied by the spring constant (N $m^{-1}$) to calculate the force (N). Most manufacturers supply a nominal spring constant for a given cantilever. The spring constant can be estimated from the dimensions of the cantilever and the properties of the constituent material. However, true spring constants of cantilevers frequently differ from the nominal values by a factor of up to 3. Most AFM software packages enable the measurement of the spring constant of a cantilever using the thermal noise method, which records the thermal fluctuations of the cantilever and uses these data in conjunction with the equipartition theorem to calculate the cantilever spring constant[111]. Essentially, the theorem equates the thermal energy at a given temperature with the energy within the oscillation of the cantilever. The thermal noise method is the most versatile and implementable method of cantilever calibration[112]. A high estimate of the method's error is 20% (ref. 112). It can be argued that other calibration methods are more accurate; however, the extra effort required to apply these with the numerous cantilevers used for these studies make them unfeasible.

**Performing a single-cell AFM mechanics experiment** ● **TIMING 1 h**
**11|** Select a mitotic cell using light microscopy by following the steps in options A or B for prophase or prometaphase/metaphase cells, respectively.

**(A) Prophase cells**

(i) Trypsinize the cells to trigger cell rounding. Use a fluorescent chromatin signal to select a prophase cell, which can be identified by condensed chromosomes inside an intact nucleus (**Fig. 4**; see ref. 85 for further details). We have successfully used histone H2B-GFP transgenic cell lines, which can be produced as outlined by Kanda *et al.*[113]. Alternatively, Hoechst 33342 (100 ng $ml^{-1}$) may be used to visualize chromatin for a short range of time[114].
▲ **CRITICAL STEP** Be careful not to excessively agitate the medium or cover slip, as this will cause trypsinized cells to dissociate from the substrate.

**(B) Prometaphase/metaphase cells**

(i) Simply identify a candidate round mitotic cell with DIC imaging. Typically dying and apoptotic cells have a distinct shriveled appearance compared with the smooth, round morphology of mitotic cells as seen with DIC imaging.

**12|** Move the cantilever onto a blank place on the glass cover slip adjacent to the cell and determine the height of the glass surface.

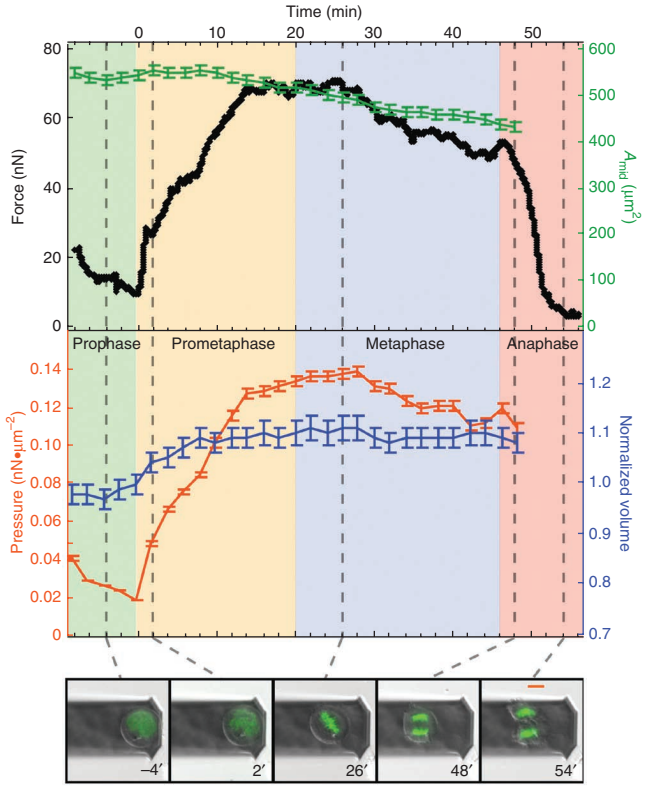


**Figure 4** | Representative force (black), cross-sectional area (green), rounding pressure (orange) and normalized volume (blue) data plots for a trypsinized cell transitioning through G2/M of the cell cycle. Gray dashed lines indicate the time of overlaid DIC and fluorescence images. Mitotic phases are: prophase (green background), prometaphase (orange background), metaphase (blue background) and anaphase (red background). Time zero denotes the transition from prophase to prometaphase, which is defined by nuclear envelope breakdown. Fluorescence images of GFP-labeled histone (H2B-GFP) were used to determine the phase of mitosis according to the following criteria: prophase cells contained condensed chromosomes surrounded by a nuclear envelope; prometaphase started with nuclear envelope breakdown; metaphase was when chromosomes aligned at the metaphase plate and in anaphase the two sets of chromosomes separated. Scale bars, 10 µm. Error bars of ±2% are based on uncertainty from DIC images.

**13|** Position the end of the cantilever over the cell. Use the AFM software to extend the cantilever until it is 8 µm above the cover slip; hold this position. The cell will now be compressed into a near-cylindrical shape (**Fig. 1b**). Use the AFM software options to stream the recorded force into a text or other data file.

▲ **CRITICAL STEP** In this protocol and the experiments of Stewart *et al.*[85], the 8-µm compression height was selected for round mitotic HeLa cells as it deforms the cell by ~50% and maintains the cell in a near-cylindrical shape, which is a convenient shape for pressure and volume calculation using top-view microscopy (**Fig. 1c**). However, the amount of deformation imposed on the cell can be tailored to the specific needs of the experiment or the cells being investigated.

**? TROUBLESHOOTING**

**14|** Use the light microscopy software to acquire DIC images of the cell at regular intervals of 2 min or to suit the requirements of the experiment. The researcher may proceed to Step 15 (to perform a medium-exchange perturbation experiment) or skip to Step 19 (to complete the single-cell AFM mechanics experiment).

▲ **CRITICAL STEP** These images can be analyzed with microscopy software to extract the contact area of the cell with the cantilever (**Fig. 1c**) and the distance ($x$) from the right side of the cell to the cantilever end (**Fig. 1c**). In conjunction with the forces measured by the AFM ($F$), these values can be used to estimate pressure and volume of the cell at the given time point (**Fig. 1d**).

**? TROUBLESHOOTING**

**Performing a medium-exchange perturbation experiment**

**15|** To perform a hypotonic shock or other medium exchange on a cell during a single-cell AFM constant-height clamp experiment, a push-pull pump can be used to exchange medium through the fluid chamber (**Fig. 1b**). Follow the pump manufacturer's instructions to ensure that the pump setup is synchronized for push-pull experiments, such that each pump pumps at the same rate in opposite directions.

**16|** Fill a 3-ml syringe with either hypotonic medium (see REAGENT SETUP) or AFM medium with EIPA (see REAGENT SETUP), connect it to the inlet tube that was set up in Step 3 and load it into the nominated 'push' pump. Load an empty 3-ml syringe into the 'pull' pump and connect it to the outlet tube.

**17|** Select a pumping speed fast enough to exchange the contents of the syringe quickly, such that hypotonic shock or other medium exchange will occur within less than 1 min. In our experiments, we exchanged volume five times at ~2,900 µl $min^{-1}$, the maximum speed that can be achieved with the BD 3-ml syringe on this apparatus.

**18|** At a convenient time in the single-cell AFM mechanics experiment, commence the pumping program to exchange the contents of the experimental chamber.

▲ **CRITICAL STEP** To prevent bubbles from being pumped into the experimental chamber, pump no more than 95% of the syringe volume into the AFM fluid chamber.

**? TROUBLESHOOTING**

**Finishing a single-cell AFM mechanics experiment**

**19|** After sufficient data have been collected on a single cell, it is often helpful to assess the extent of drift in the experimental setup. Without moving the AFM head vertically, remeasure the height of the glass cover slip and compare it with what was measured in Step 12. If the glass surface–to–AFM head drift is excessive (>1 μm $h^{-1}$), this must be taken into account when reviewing the data.

**? TROUBLESHOOTING**

**20|** Exchange the medium in the experimental chamber with normal AFM medium to get back to the starting point for another single-cell experiment. Allow the cells 20 min to adjust before recommencing measurements. *Note*: This duration may depend on the cell type.

▲ **CRITICAL STEP** The effect of some perturbations or drugs is not quickly reversible, and therefore it may be more advantageous to bring in a new sample of cells for subsequent experiments. To do this, complete Step 4 and then skip straight to Step 11.

**21|** Once all experiments are completed for the day, remove the AFM head from the stage, disassemble the fluid chamber and dismount the cantilever holder from the AFM head. Because the cantilever and cantilever holder are in contact with medium containing 10% (vol/vol) FBS, they tend to become caked with proteins but can be effectively cleaned with 2–5% (vol/vol) Helmanex in ultrasonic conditions. Well-cleaned cantilevers can be reused.

**? TROUBLESHOOTING**

**Problem: excessive evaporation of cell medium**

This may be detrimental to cell viability and cause problems such as limited passage through the cell cycle.

*Solution*: ensure that the appropriate seals are correctly in place.

*Steps*: the problem may affect any Step from 11 to 18 and may originate in Step 3 or 4.

**Problem: periodic deviations in measured force not related to the cell mechanics are occurring**

*Possible reasons*: debris in the cell medium is floating in the path of the laser. Periodic releases in tension between the cover slip and fluid chamber seals trigger mechanical instabilities in the setup.

*Solution*: prerinsing the cells with PBS before adding cell medium can reduce debris. To eliminate periodic force spikes caused by an unstable contact between the cover slip and fluid chamber seal, ensure that the seal is flush with the glass cover slip and is not either stretched or crinkled in any way.

*Steps*: the problem becomes apparent in Steps 13 and 14; it originates in Step 4.

**Problem: the cells slide up the cantilever gradient**

*Possible reason*: the cells have too little adhesion to the glass cover slip. Combined with the 10° angle of the cantilever, this will cause sliding of the cells up the cantilever as soon as cells exert a sufficiently high force against the cantilever.

*Solution*: attempt to choose a candidate mitotic cell adjacent to a flat adherent cell on the appropriate side of the mitotic cell. The flat adherent cell will usually stop the round cell from sliding. Currently, we are working on a cantilever design to provide proper parallel plate mechanics and eliminate this inconvenience.

*Steps*: the problem becomes apparent in Steps 13 and 14; the problem may originate in Step 11.

**Problem: deviations in measured force occurs upon medium exchange**

*Possible reason*: the refractive indices of the solutions are not balanced.

*Solution*: use a refractometer to confirm the refractive indices of medium samples before commencing exchange. Add Ficoll, as appropriate, at +0.0013 RI per 1% (wt/vol) in order to match the medium (see REAGENT SETUP).

*Step*: the problem becomes apparent in Step 18.

**Problem: the cantilever–cover slip distance is drifting excessively**

*Possible reason*: the setup is not thermally equilibrated.

*Solution*: as a permanent solution, we use and recommend a temperature control system that hosts the entire AFM and optical microscopy setup, buffer solutions and pipettes, and which holds the temperature (for example) at 37 °C (e.g., Cube + Box). Otherwise, ensure that the environment/room has a well-controlled temperature and allow the setup to equilibrate for longer times before beginning experiments. It may be beneficial to start up the equipment several hours before beginning the experiment.

*Step*: the problem becomes apparent in Step 19.

**Problem: cell-cell variability makes it difficult to gauge trends**

*Possible reason*: the number of cells used is not sufficient to get statistically meaningful information.

*Solution*: a minimum of 5–10 cells is often needed to make robust conclusions.

*Steps*: Steps 11–19 must be repeated sufficient times for each condition.

## ● TIMING

Steps 1–10, AFM setup: 1 h

Steps 11–20, AFM constant-height clamp and medium-exchange experiment on a single cell: 1 h

## ANTICIPATED RESULTS

Here we use this protocol to monitor two different categories of mechanical transitions in mitotic cells. The first is due to intrinsic signals that direct the cell through the cell cycle from G2 into mitosis (**Fig. 4**). The second is due to extrinsically imposed perturbations that can either be physical, such as a hypotonic shock (**Fig. 5a**), or biochemical, such as exposure to the chemical inhibitor, EIPA, which blocks the $Na^+/H^+$ antiporter NHE1[110] (**Fig. 5b**). To exemplify data analysis and presentation, we use a twin panel format with force (black) and cross-sectional area (green) on top, and normalized volume (blue) and pressure (orange) below. The position of the cell with respect to the cantilever edge, *x* (**Fig. 1**), is not plotted but is used in subsequent calculations (**Fig. 1c**,**d**).

**Figure 4** shows the protocol being applied to a trypsinized prophase cell. The mitotic state of the cell is first identified by fluorescence imaging of chromatin (H2B-GFP); the protocol must be launched quickly as condensed chromosomes may only be visible for a limited duration. As the cell transitions into mitosis at nuclear envelope breakdown, it markedly increases its resistance pressure against the cantilever. One inconvenience to be aware of is that cells may sometimes slide along the tilted cantilever (see TROUBLESHOOTING).

**Figure 5a** shows a prometaphase/metaphase cell subjected to hypotonic shock. Water flows into the cell, which leads to an increase in cell volume and pressure. The cell responds by rapidly activating transporters at the plasma membrane to affect the efflux of osmolytes and bring intracellular volume and pressure close to previous levels in a process known as regulatory volume decrease[115]. To properly track the dynamics of this process, we acquired DIC images every 20 s during perturbation and regulatory volume decrease. This is an example where it was necessary to tailor the data collection

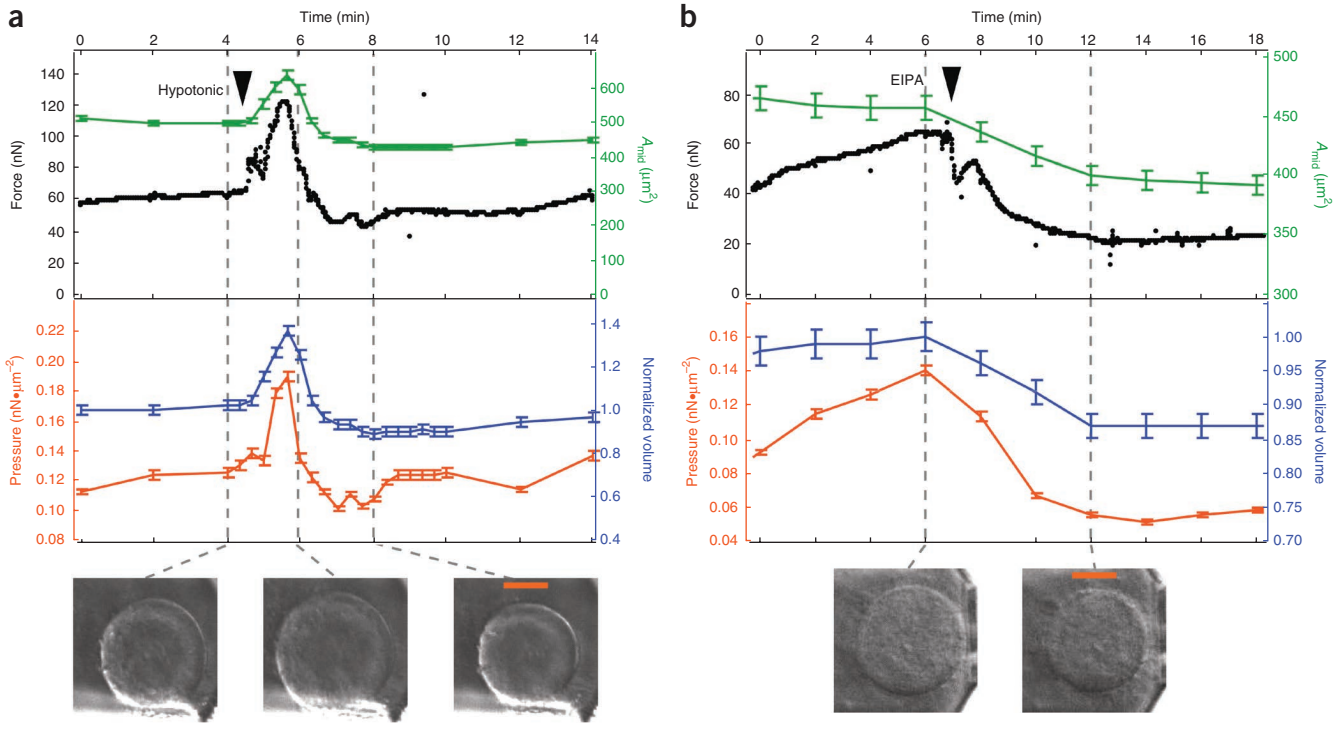


**Figure 5** | Representative force (black), cross-sectional area (green), rounding pressure (orange) and normalized volume (blue) plots for cells. (**a**,**b**) Cells were subjected to a hypotonic treatment (−Δ100 mOsm per liter) medium (**a**) and 50 μM EIPA (5-(*N*-ethyl-*N*-isopropyl)amiloride) (**b**) as indicated by a black arrow. Error bars (± 2%) are based on the measurement uncertainty carried through from DIC measurements. Experiments were conducted in the prometaphase/metaphase segment of mitosis. Time zero represents at arbitrary time in prometaphase a few minutes after the protocol was launched. Gray dashed lines indicate the time of DIC images. Scale bars, 10 μm.

rationale to the needs of the experiment. Interestingly, other reports[116] indicate that the regulatory volume decrease of uncompressed HeLa cells may be substantially slower. Thus, our assay provides a useful way to study the effect of compressive pressure on volume regulation, as both parameters can be measured simultaneously. Moreover, as cells in real tissue are subject to the stresses and strains of a 3D environment, one may use this protocol to mimic natural forces and study their effect on volume regulation. **Figure 5b** shows anticipated results when exposing compressed mitotic cells to the $Na^+/H^+$ antiporter NHE1 inhibitor EIPA (**Fig. 5b**). The figure reveals that cellular pressure and volume both decrease substantially within several minutes of $Na^+/H^+$ exchange inhibition. To obtain enough statistical information to sufficiently gauge trends, we recommend a minimum of five cells per condition (see TROUBLESHOOTING).

**ACKNOWLEDGMENTS** We thank J. Helenius for stimulatory discussions and advice, and J. Howard for advice on refractive index change during medium exchange. This work was supported by the Bundesministerium für Bildung und Forschung (BMBF), the Swiss National Center of Competence in Research (NCCR) "Nanoscale Science", the Max Planck Society and the Japan Society for the Promotion of Science (JSPS).

**AUTHOR CONTRIBUTIONS** M.P.S. and D.J.M. designed the AFM protocol, and Y.T. devised its application to mitotic cells. M.P.S. performed and optimized the experimental procedure. M.P.S., A.A.H., Y.T. and D.J.M. contributed to the manuscript.

**COMPETING FINANCIAL INTERESTS** The authors declare no competing financial interests.

Published online at http://www.natureprotocols.com/.
Reprints and permissions information is available online at http://www.nature.com/reprints/index.html.

1. Eggert, U.S., Mitchison, T.J. & Field, C.M. Animal cytokinesis: from parts list to mechanisms. *Annu. Rev. Biochem.* **75**, 543–566 (2006).
2. Robinson, D.N. & Spudich, J.A. Mechanics and regulation of cytokinesis. *Curr. Opin. Cell. Biol.* **16**, 182–188 (2004).
3. Discher, D.E., Mooney, D.J. & Zandstra, P.W. Growth factors, matrices, and forces combine and control stem cells. *Science* **324**, 1673–1677 (2009).
4. Guck, J., Lautenschlager, F., Paschke, S. & Beil, M. Critical review: cellular mechanobiology and amoeboid migration. *Integr. Biol. (Camb.)* **2**, 575–583 (2010).
5. Lammermann, T. & Sixt, M. Mechanical modes of 'amoeboid' cell migration. *Curr. Opin. Cell. Biol.* **21**, 636–644 (2009).
6. Gardel, M.L., Schneider, I.C., Aratyn-Schaus, Y. & Waterman, C.M. Mechanical integration of actin and adhesion dynamics in cell migration. *Annu. Rev. Cell. Dev. Biol.* **26**, 315–333 (2010).
7. Bryant, D.M. & Mostov, K.E. From cells to organs: building polarized tissue. *Nat. Rev. Mol. Cell. Biol.* **9**, 887–901 (2008).
8. Mammoto, T. & Ingber, D.E. Mechanical control of tissue and organ development. *Development* **137**, 1407–1420 (2010).
9. von Dassow, M. & Davidson, L.A. Variation and robustness of the mechanics of gastrulation: the role of tissue mechanical properties during morphogenesis. *Birth Defects Res. C. Embryo. Today* **81**, 253–269 (2007).
10. Paluch, E. & Heisenberg, C.P. Biology and physics of cell shape changes in development. *Curr. Biol.* **19**, R790–R799 (2009).
11. Grinnell, F. & Petroll, W.M. Cell motility and mechanics in three-dimensional collagen matrices. *Annu. Rev. Cell. Dev. Biol.* **26**, 335–361 (2010).
12. Butcher, D.T., Alliston, T. & Weaver, V.M. A tense situation: forcing tumour progression. *Nat. Rev. Cancer* **9**, 108–122 (2009).
13. Provenzano, P.P. & Keely, P.J. Mechanical signaling through the cytoskeleton regulates cell proliferation by coordinated focal adhesion and Rho GTPase signaling. *J. Cell. Sci.* **124**, 1195–1205 (2011).
14. Wyss, H.M. *et al.* Biophysical properties of normal and diseased renal glomeruli. *Am. J. Physiol. Cell. Physiol.* **300**, C397–C405 (2011).
15. Lombardi, M.L. & Lammerding, J. Altered mechanical properties of the nucleus in disease. *Meth. Cell. Biol.* **98**, 121–141 (2010).
16. Discher, D. *et al.* Biomechanics: cell research and applications for the next decade. *Ann. Biomed. Eng.* **37**, 847–859 (2009).
17. Remmerbach, T.W. *et al.* Oral cancer diagnosis by mechanical phenotyping. *Cancer Res.* **69**, 1728–1732 (2009).
18. Fabry, B. & Fredberg, J.J. Mechanotransduction, asthma, and airway smooth muscle. *Drug Discov. Today Dis. Models* **4**, 131–137 (2007).
19. Janmey, P.A. & Miller, R.T. Mechanisms of mechanical signaling in development and disease. *J. Cell. Sci.* **124**, 9–18 (2011).
20. Cheng, G., Tse, J., Jain, R.K. & Munn, L.L. Micro-environmental mechanical stress controls tumor spheroid size and morphology by suppressing proliferation and inducing apoptosis in cancer cells. *PLoS One* **4**, e4632 (2009).
21. Lee, G.Y.H. & Lim, C.T. Biomechanics approaches to studying human diseases. *Trends Biotechnol.* **25**, 111–118 (2007).
22. Wang, J.H. & Li, B. Mechanics rules cell biology. *Sports Med. Arthrosc. Rehabil. Ther. Technol.* **2**, 16 (2010).
23. Vogel, V. & Sheetz, M. Local force and geometry sensing regulate cell functions. *Nat. Rev. Mol. Cell. Biol.* **7**, 265–275 (2006).
24. Janmey, P.A., Georges, P.C. & Hvidt, S. Basic rheology for biologists. *Meth. Cell. Biol.* **83**, 3–27 (2007).
25. Pelling, A.E. & Horton, M.A. An historical perspective on cell mechanics. *Pflugers. Arch.* **456**, 3–12 (2008).
26. Vlès, F. Les tensions de surface et les deformations de l'oeuf d'oursin. *Arch. de Phys. Biol.* **4**, 263–284 (1926).
27. Harvey, E.N. & Loomis, A.L. A microscope-centrifuge. *Science* **72**, 42–44 (1930).
28. Hiramoto, Y. Observations and measurements of sea urchin eggs with a centrifuge microscope. *J. Cell. Physiol.* **69**, 219–230 (1967).
29. Cole, K.S. Surface forces of the arbacia egg. *J. Cell. Comp. Physiol.* **1**, 1–9 (1932).
30. Hiramoto, Y. Mechanical properties of sea urchin eggs. I. Surface force and elastic modulus of the cell membrane. *Exp. Cell. Res.* **32**, 59–75 (1963).
31. Yoneda, M. & Dan, K. Tension at the surface of the dividing sea-urchin egg. *J. Exp. Biol.* **57**, 575–587 (1972).
32. Wolpert, L. Mechanical properties of membrane of sea urchin egg during cleavage. *Exp. Cell. Res.* **41**, 385–396 (1966).
33. Mitchison, J.M. & Swann, M.M. The mechanical properties of the cell surface. 1. The cell elastimeter. *J. Exp. Biol.* **31**, 443 (1954).
34. Rappaport, R. Cell division—direct measurement of maximum tension exerted by furrow of echindoerm eggs. *Science* **156**, 1241–1243 (1967).
35. Rappaport, R. Cleavage of sand dollar eggs under constant tensile stress. *J. Exp. Zool.* **144**, 225–231 (1960).
36. Rand, R.P. & Burton, A.C. Mechanical properties of the red cell membrane. I. Membrane stiffness and intracellular pressure. *Biophys. J.* **4**, 115–135 (1964).
37. Evans, E.A. & Lacelle, P.L. Intrinsic material properties of erythrocyte-membrane indicated by mechanical analysis of deformation. *Blood* **45**, 29–43 (1975).
38. Hochmuth, R.M. & Mohandas, N. Uniaxial loading of red-cell membrane. *J. Biomech.* **5**, 501–509 (1972).
39. Weed, R.I., Lacelle, P.L. & Merrill, E.W. Metabolic dependence of red cell deformability. *J. Clin. Invest.* **48**, 795–809 (1969).
40. Klug, P.P., Lessin, L.S. & Radice, P. Rheological aspects of sickle-cell disease. *Arch. Intern. Med.* **133**, 577–590 (1974).
41. Suresh, S. *et al.* Connections between single-cell biomechanics and human disease states: gastrointestinal cancer and malaria. *Acta. Biomater.* **1**, 15–30 (2005).
42. Skalak, R. Biomechanics at the cellular-level—the Alza distinguished lecture. *Ann. Biomed. Eng.* **12**, 305–318 (1984).
43. Muller, D.J., Helenius, J., Alsteens, D. & Dufrene, Y.F. Force probing surfaces of living cells to molecular resolution. *Nat. Chem. Biol.* **5**, 383–390 (2009).
44. Hochmuth, R.M. Micropipette aspiration of living cells. *J. Biomech.* **33**, 15–22 (2000).
45. Thoumine, O. & Ott, A. Time scale dependent viscoelastic and contractile regimes in fibroblasts probed by microplate manipulation. *J. Cell. Sci.* **110**, 2109–2116 (1997).

46. Mitrossilis, D. *et al.* Single-cell response to stiffness exhibits muscle-like behavior. *Proc. Natl. Acad. Sci. USA* **106**, 18243–18248 (2009).
47. Fabry, B. *et al.* Selected contribution: time course and heterogeneity of contractile responses in cultured human airway smooth muscle cells. *J. Appl. Physiol.* **91**, 986–994 (2001).
48. Wang, N., Butler, J.P. & Ingber, D.E. Mechanotransduction across the cell-surface and through the cytoskeleton. *Science* **260**, 1124–1127 (1993).
49. Kasza, K.E., Vader, D., Koster, S., Wang, N. & Weitz, D.A. Magnetic twisting cytometry. *Cold Spring Harb. Protoc.* published online, doi:10.1101/pdb.prot5599 (1 April 2011).
50. Zhang, H. & Liu, K.K. Optical tweezers for single cells. *JR Soc. Interface* **5**, 671–690 (2008).
51. Ou-Yang, H.D. & Wei, M.T. Complex fluids: probing mechanical properties of biological systems with optical tweezers. *Annu. Rev. Phys. Chem.* **61**, 421–440 (2010).
52. Mizuno, D., Bacabac, R., Tardin, C., Head, D. & Schmidt, C.F. High-resolution probing of cellular force transmission. *Phys. Rev. Lett.* **102**, 168102 (2009).
53. Lincoln, B., Wottawah, F., Schinkinger, S., Ebert, S. & Guck, J. High-throughput rheological measurements with an optical stretcher. *Meth. Cell. Biol.* **83**, 397–423 (2007).
54. Knezevic, V., Sim, A.J., Borg, T.K. & Holmes, J.W. Isotonic biaxial loading of fibroblast-populated collagen gels: a versatile, low-cost system for the study of mechanobiology. *Biomech. Model. Mechanobiol.* **1**, 59–67 (2002).
55. Sotoudeh, M., Jalali, S., Usami, S., Shyy, J.Y. & Chien, S. A strain device imposing dynamic and uniform equi-biaxial strain to cultured cells. *Ann. Biomed. Eng.* **26**, 181–189 (1998).
56. Young, E.W.K., Wheeler, A.R. & Simmons, C.A. Matrix-dependent adhesion of vascular and valvular endothelial cells in microfluidic channels. *Lab. Chip.* **7**, 1759–1766 (2007).
57. Malek, A.M. & Izumo, S. Mechanism of endothelial cell shape change and cytoskeletal remodeling in response to fluid shear stress. *J. Cell. Sci.* **109**, 713–726 (1996).
58. Gabriele, S., Benoliel, A.M., Bongrand, P. & Theodoly, O. Microfluidic investigation reveals distinct roles for actin cytoskeleton and myosin II activity in capillary leukocyte trafficking. *Biophys. J.* **96**, 4308–4318 (2009).
59. Rosenbluth, M.J., Lam, W.A. & Fletcher, D.A. Analyzing cell mechanics in hematologic diseases with microfluidic biophysical flow cytometry. *Lab. Chip.* **8**, 1062–1070 (2008).
60. Siechen, S., Yang, S.Y., Chiba, A. & Saif, T. Mechanical tension contributes to clustering of neurotransmitter vesicles at presynaptic terminals. *Proc. Natl. Acad. Sci. USA* **106**, 12611–12616 (2009).
61. Loh, O., Vaziri, A. & Espinosa, H.D.S.M. The potential of MEMS for advancing experiments and modeling in cell mechanics. *Exp. Mech.* **49**, 105–124 (2009).
62. Radmacher, M. Studying the mechanics of cellular processes by atomic force microscopy. *Meth. Cell. Biol.* **83**, 347–372 (2007).
63. Mahaffy, R.E., Shih, C.K., MacKintosh, F.C. & Kas, J. Scanning probe-based frequency-dependent microrheology of polymer gels and biological cells. *Phys. Rev. Lett.* **85**, 880–883 (2000).
64. Alcaraz, J. *et al.* Correction of microrheological measurements of soft samples with atomic force microscopy for the hydrodynamic drag on the cantilever. *Langmuir* **18**, 716–721 (2002).
65. Smith, B.A., Tolloczko, B., Martin, J.G. & Grutter, P. Probing the viscoelastic behavior of cultured airway smooth muscle cells with atomic force microscopy: stiffening induced by contractile agonist. *Biophys. J.* **88**, 2994–3007 (2005).
66. Gavara, N. & Chadwick, R.S. Noncontact microrheology at acoustic frequencies using frequency-modulated atomic force microscopy. *Nat. Methods* **7**, 650–654 (2010).
67. Lam, W.A. *et al.* Mechanics and contraction dynamics of single platelets and implications for clot stiffening. *Nat. Mater.* **10**, 61–66 (2011).
68. Brangwynne, C.P., MacKintosh, F.C. & Weitz, D.A. Force fluctuations and polymerization dynamics of intracellular microtubules. *Proc. Natl. Acad. Sci. USA* **104**, 16128–16133 (2007).
69. Park, K. *et al.* Measurement of adherent cell mass and growth. *Proc. Natl. Acad. Sci. USA* **107**, 20691–20696 (2010).
70. Sen, S. & Kumar, S. Cell-matrix de-adhesion dynamics reflect contractile mechanics. *Cell. Mol. Bioeng.* **2**, 218–230 (2009).
71. Wildt, B., Wirtz, D. & Searson, P.C. Triggering cell detachment from patterned electrode arrays by programmed subcellular release. *Nat. Protoc.* **5**, 1273–1280 (2010).
72. Thomas, A. *et al.* Real-time elastography—an advanced method of ultrasound: first results in 108 patients with breast lesions. *Ultrasound Obstet. Gynecol.* **28**, 335–340 (2006).
73. Kundu, T., Bereiter-Hahn, J. & Hillmann, K. Measuring elastic properties of cells by evaluation of scanning acoustic microscopy V(Z) values using simplex algorithm. *Biophys. J.* **59**, 1194–1207 (1991).
74. Mayer, M., Depken, M., Bois, J.S., Julicher, F. & Grill, S.W. Anisotropies in cortical tension reveal the physical basis of polarizing cortical flows. *Nature* **467**, 617–621 (2010).
75. Ji, L., Loerke, D., Gardel, M. & Danuser, G. Probing intracellular force distributions by high-resolution live cell imaging and inverse dynamics. *Meth. Cell. Biol.* **83**, 199–235 (2007).
76. Dembo, M. & Wang, Y.L. Stresses at the cell-to-substrate interface during locomotion of fibroblasts. *Biophys. J.* **76**, 2307–2316 (1999).
77. Lee, J. The use of gelatin substrates for traction force microscopy in rapidly moving cells. *Meth. Cell. Biol.* **83**, 297–312 (2007).
78. Tan, J.L. *et al.* Cells lying on a bed of microneedles: an approach to isolate mechanical force. *Proc. Natl. Acad. Sci. USA* **100**, 1484–1489 (2003).
79. Yang, M.T., Fu, J., Wang, Y.K., Desai, R.A. & Chen, C.S. Assaying stem cell mechanobiology on microfabricated elastomeric substrates with geometrically modulated rigidity. *Nat. Protoc.* **6**, 187–213 (2011).
80. Maskarinec, S.A., Franck, C., Tirrell, D.A. & Ravichandran, G. Quantifying cellular traction forces in three dimensions. *Proc. Natl. Acad. Sci. USA* **106**, 22108–22113 (2009).
81. Legant, W.R. *et al.* Measurement of mechanical tractions exerted by cells in three-dimensional matrices. *Nat. Methods* **7**, 969–971 (2010).
82. Dimitriadis, E.K., Horkay, F., Maresca, J., Kachar, B. & Chadwick, R.S. Determination of elastic moduli of thin layers of soft material using the atomic force microscope. *Biophys. J.* **82**, 2798–2810 (2002).
83. Rosenbluth, M.J., Lam, W.A. & Fletcher, D.A. Force microscopy of nonadherent cells: a comparison of leukemia cell deformability. *Biophys. J.* **90**, 2994–3003 (2006).
84. Krieg, M. *et al.* Tensile forces govern germ-layer organization in zebrafish. *Nat. Cell. Biol.* **10**, 429–436 (2008).
85. Stewart, M.P. *et al.* Hydrostatic pressure and the actomyosin cortex drive mitotic cell rounding. *Nature* **469**, 226–230 (2011).
86. Webster, K.D., Crow, A. & Fletcher, D.A. An AFM-based stiffness clamp for dynamic control of rigidity. *PLoS One* **6**, e17807 (2011).
87. Chaudhuri, O., Parekh, S.H. & Fletcher, D.A. Reversible stress softening of actin networks. *Nature* **445**, 295–298 (2007).
88. Friedrichs, J., Helenius, J. & Muller, D.J. Quantifying cellular adhesion to extracellular matrix components by single-cell force spectroscopy. *Nat. Protoc.* **5**, 1353–1361 (2010).
89. Helenius, J., Heisenberg, C.P., Gaub, H.E. & Muller, D.J. Single-cell force spectroscopy. *J. Cell. Sci.* **121**, 1785–1791 (2008).
90. Prass, M., Jacobson, K., Mogilner, A. & Radmacher, M. Direct measurement of the lamellipodial protrusive force in a migrating cell. *J. Cell. Biol.* **174**, 767–772 (2006).
91. Muller, D.J. & Dufrene, Y.F. Atomic force microscopy as a multifunctional molecular toolbox in nanobiotechnology. *Nat. Nanotechnol.* **3**, 261–269 (2008).
92. Stewart, M.P., Toyoda, Y., Hyman, A.A. & Muller, D.J. Force probing cell shape changes to molecular resolution. *Trends. Biochem. Sci.* **36**, 444–450 (2011).
93. Carreno, S. *et al.* Moesin and its activating kinase Slik are required for cortical stability and microtubule organization in mitotic cells. *J. Cell. Biol.* **180**, 739–746 (2008).
94. Cramer, L.P. & Mitchison, T.J. Investigation of the mechanism of retraction of the cell margin and rearward flow of nodules during mitotic cell rounding. *Mol. Biol. Cell.* **8**, 109–119 (1997).
95. Kunda, P., Pelling, A.E., Liu, T. & Baum, B. Moesin controls cortical rigidity, cell rounding, and spindle morphogenesis during mitosis. *Curr. Biol.* **18**, 91–101 (2008).
96. Maddox, A.S. & Burridge, K. RhoA is required for cortical retraction and rigidity during mitotic cell rounding. *J. Cell. Biol.* **160**, 255–265 (2003).
97. Radmacher, M., Fritz, M. & Hansma, P.K. Imaging soft samples with the atomic-force microscope—gelatin in water and propanol. *Biophys. J.* **69**, 264–270 (1995).
98. Hertz, H. Uber den Kontakt elastischer Korper. *J. Reine. Angew. Mathematik.* **92**, 156–188 (1881).
99. Sneddon, I. The relation between load and penetration in the axisymmetric boussinesq problem for a punch of arbitrary profile. *Int. J. Eng. Sc.* **3**, 47–57 (1965).
100. Radmacher, M., Fritz, M., Kacher, C.M., Cleveland, J.P. & Hansma, P.K. Measuring the viscoelastic properties of human platelets with the atomic force microscope. *Biophys. J.* **70**, 556–567 (1996).
101. Quist, A.P., Rhee, S.K., Lin, H. & Lal, R. Physiological role of gap-junctional hemichannels. Extracellular calcium-dependent isosmotic volume regulation. *J. Cell. Biol.* **148**, 1063–1074 (2000).
102. Schneider, S.W., Matzke, R., Radmacher, M. & Oberleithner, H. Shape and volume of living aldosterone-sensitive cells imaged with the atomic force microscope. *Meth. Mol. Biol.* **242**, 255–279 (2004).

103. Harris, A.R. & Charras, G.T. Experimental validation of atomic force microscopy-based cell elasticity measurements. *Nanotechnology* **22**, 345102 (2011).
104. Callies, C. *et al.* Membrane potential depolarization decreases the stiffness of vascular endothelial cells. *J. Cell. Sci.* **124**, 1936–1942 (2011).
105. Jin, L.W., Lulevich, V., Zimmer, C.C., Hong, H.S. & Liu, G.Y. Single-cell mechanics provides a sensitive and quantitative means for probing amyloid-beta peptide and neuronal cell interactions. *Proc. Natl. Acad. Sci. USA* **107**, 13872–13877 (2010).
106. Zhou, E.H. *et al.* Universal behavior of the osmotically compressed cell and its analogy to the colloidal glass transition. *Proc. Natl. Acad. Sci. USA* **106**, 10632–10637 (2009).
107. Spagnoli, C., Beyder, A., Besch, S. & Sachs, F. Atomic force microscopy analysis of cell volume regulation. *Phys. Rev. E. Stat. Nonlin. Soft. Matter Phys.* **78**, 031916 (2008).
108. Steltenkamp, S., Rommel, C., Wegener, J. & Janshoff, A. Membrane stiffness of animal cells challenged by osmotic stress. *Small* **2**, 1016–1020 (2006).
109. Salbreux, G., Joanny, J.F., Prost, J. & Pullarkat, P. Shape oscillations of non-adhering fibroblast cells. *Phys. Biol.* **4**, 268–284 (2007).
110. Vigne, P., Frelin, C., Cragoe, E.J., Jr. & Lazdunski, M. Ethylisopropyl-amiloride: a new and highly potent derivative of amiloride for the inhibition of the Na+/H+ exchange system in various cell types. *Biochem. Biophys. Res. Commun.* **116**, 86–90 (1983).
111. Hutter, J.L. & Bechhoefer, J. Calibration of atomic-force microscope tips. *Rev. Sci. Instr.* **64**, 1868–1873 (1993).
112. Burnham, N.A. *et al.* Comparison of calibration methods for atomic-force microscopy cantilevers. *Nanotechnology* **14**, 1–6 (2003).
113. Kanda, T., Sullivan, K.F. & Wahl, G.M. Histone-GFP fusion protein enables sensitive analysis of chromosome dynamics in living mammalian cells. *Curr. Biol.* **8**, 377–385 (1998).
114. Haraguchi, T., Kaneda, T. & Hiraoka, Y. Dynamics of chromosomes and microtubules visualized by multiple-wavelength fluorescence imaging in living mammalian cells: effects of mitotic inhibitors on cell cycle progression. *Genes Cells* **2**, 369–380 (1997).
115. Lang, F. *Mechanisms and Significance of Cell Volume Regulation* (Karger, 2006).
116. Numata, T., Shimizu, T. & Okada, Y. TRPM7 is a stretch- and swelling-activated cation channel involved in volume regulation in human epithelial cells. *Am. J. Physiol-Cell. Ph.* **292**, C460–C467 (2007).